Excited State Resonance Raman of Flavin Mononucleotide: Comparison of Theory and Experiment

Dale Green,[1] Palas Roy,[1] Christopher R. Hall,[1‡] James N. Iuliano,[2] Garth A. Jones,[1] Andras Lukacs,[3] Peter J. Tonge[2]* and Stephen R. Meech[1]*

[1]*School of Chemistry, University of East Anglia, Norwich NR4 7TJ, U.K.,* [2]*Department of Chemistry, Stony Brook University, Stony Brook, New York 11794-3400, United States,* [3]*Department of Biophysics, Medical School, University of Pecs, Szigeti ut 12, 7624 Pecs, Hungary*

Abstract

Blue light absorbing flavoproteins play important roles in a variety of photobiological processes. Consequently, there have been numerous investigations of their excited state structure and dynamics, in particular by time resolved vibrational spectroscopy. The isoalloxazine chromophore of the flavoprotein co-factors has been studied in detail by time resolved Raman, lending it a benchmark status for mode assignments in excited electronic states of large molecules. However, detailed comparisons of calculated and measured spectra have proven challenging, as there are many more modes calculated than are observed, and the role of resonance enhancement is difficult to characterise in excited electronic states. Here we employ a recently developed approach due to Elles and co-workers. (*J. Phys. Chem. A* **2018**, *122*, 8308–8319) for the calculation of resonance enhanced Raman spectra of excited states, and apply it to the lowest singlet and triplet excited states of the isoalloxazine chromophore. There is generally good agreement between calculated and observed enhancements, which allows assignment of vibrational bands of the flavoprotein co-factors to be refined. However, some prominently enhanced bands are found to be absent from the calculations, suggesting the need for further development of the theory.

*Address for correspondence: peter.tonge@stonybrook.edu; s.meech@uea.ac.uk

[‡]Present address: School of Chemistry, 153, The University of Melbourne, Masson Rd, Parkville VIC 3052, Australia

Introduction

Flavoproteins play a key role in biochemistry because the flavin cofactor can access a range of oxidation and protonation states, allowing the proteins to participate in a variety of redox reactions.[1] The co-factor (Flavin Mononucleotide, FMN, or Flavin Adenine Dinucleotide, FAD) gives these proteins their yellow colour, which arises from their common isoalloxazine chromophore, which absorbs at around 450 nm. Over the past thirty years a number of flavoproteins have been shown to play an important role in photobiology.[2-3] Three families of photoactive flavoproteins have been identified, the blue light using flavin (BLUF) domain proteins,[4] the light-oxygen-voltage (LOV) domain proteins[5-7] and the photolyase/cryptochromes.[8] These are the light sensing elements in an array of photobiological functions, playing a role in processes ranging from phototaxis to circadian rhythms. Several photoactive flavoproteins function by controlling gene expression in response to light, a property which has recently been recruited in optogenetics applications.[9]

The obvious importance of isoalloxazine excited state chemistry has stimulated a number of investigations. Both optical and infra-red spectroscopy have been applied to probe flavin photochemistry in all of its accessible charge states.[10-13] These studies have been extended to photoactive flavoproteins, and the effects of optical excitation on their structure and excited state dynamics have been investigated by crystallography, NMR and pump-probe spectroscopy respectively.[14-22] These experiments have been complemented by quantum chemical calculations.[23-27] Time resolved infra-red (TRIR) spectroscopy in particular has proven a useful probe of flavin excited state reactions, and their effect on the surrounding protein matrix.[28-34] However, TRIR measurements of flavoproteins have significant drawbacks. First, measurements must be made in D_2O buffer, as H_2O absorbs strongly in the characteristic protein amide and sideband region. Second, it cannot be applied to large complexes, due to strong absorption by amide modes. Finally, TRIR difference spectra are often complicated and difficult to interpret, involving contributions from both the chromophore and the surrounding protein matrix.[35]

In contrast, transient Raman spectroscopy can be applied in aqueous solutions and to proteins of any size, limited only by their solubility. Further, resonance enhancements can be exploited, yielding simpler state specific vibrational data. However, the application of Raman in time resolved photobiology has been restricted by the twin problems of strong background fluorescence and the weakness of the signal that can be generated from transient states. These problems can to a large extent be overcome by femtosecond stimulated Raman spectroscopy (FSRS). FSRS is a coherent multipulse experiment which yields well resolved Raman spectra of resonant excited states with good signal to noise and ultrafast (sub 100 fs) time resolution. The FSRS experiment has been described in detail elsewhere.[36-37]

Weigel and co-workers reported the first FSRS spectrum of the singlet excited states of solutions of riboflavin and FAD.[38] They assigned the observed excited state Raman spectra with the aid of TDDFT calculations, and contrasted them with ground state measurements. Hall and co-workers extended the FSRS method to probe FAD in photoactive flavoproteins, and showed that the excited state spectra were sensitive to the protein environment.[39] Recently, two further FSRS studies have investigated excited states of FMN. Andrikopoulos et al probed singlet and triplet states of FMN in solution, and assigned them on the basis of TDDFT calculation.[40] Iuliano et al also reported singlet and triplet state FSRS, and presented a detailed assignment based on the study of a series of FMN isotopologues, both experimentally and through TDDFT, in solution and in LOV domain proteins.[41] As a result of these quite extensive studies, the chromophore of the flavoproteins, isoalloxazine, has one of the best characterised excited state spectra, giving it the status of a benchmark for assignment of excited state vibrations of large molecules, in addition to its established role in photobiology.

The experimental FSRS spectra of S_1 and T_1 isoalloxazines map well onto the results of TDDFT calculations. However, many more modes are found in the calculated spectrum than appear in the experiment. Typically, only five or six bands appear in the FSRS spectrum measured in the fingerprint (1100 – 1800 cm^{-1}) region of isoalloxazine, and in many cases these can plausibly be assigned to several different nearby calculated modes.[38, 40-41] With the aid of spectra from isotopologues it proved possible

to assign some experimental bands to specific modes, but in other cases multiple possible assignments remained.[41] The reason for the relative simplicity of the FSRS spectrum, compared to the calculation, is that FSRS is resonantly enhanced. It is well established that resonance enhancements simplify ground state Raman spectra, as has also been shown for isoalloxazines.[42-43] The challenge with excited state resonant FSRS spectra is that while the spectra represent the lowest excited states of most interest (S_1, T_1) the factors controlling the enhancement rests with the properties of the upper (S_n, T_n, n>1) states. Recently Elles and co-workers established that this can play a major role in FSRS spectra, and made important progress in developing and testing methods for calculating resonance enhanced FSRS.[44-45] Given the importance of the flavin co-factors in photobiology, and the benchmark status of isoalloxazine emerging from the multiple observations of its excited state Raman spectra, we have applied the approach described by Elles to model the FSRS of S_1 and T_1 isoalloxazine.

Theory

Strong enhancement of a mode in a resonance Raman spectrum is a result of the equilibrium geometry of the resonant, upper, electronic state, $|N\rangle$, being displaced with respect to that of the lower electronic state, $|I\rangle$.[46] This gives rise to significant wavefunction overlap in the Franck-Condon factors $\langle \nu_f | \nu_n \rangle$ and $\langle \nu_n | \nu_i \rangle$, between the vibrational levels of the upper state, $|\nu_n\rangle$, and the initial and final vibrational levels of the lower electronic state, $|\nu_i\rangle$ and $|\nu_f\rangle$. As described by Elles *et al.*, the intensity of the kth mode of the lower electronic state, I_k, is proportional to the square of its polarizability tensor, α_{fi}^k, which can be determined using the semiclassical gradient approximation.[44] This accounts for the vibrational overlap by propagating an initially Gaussian wavepacket on the potential energy surface of the upper electronic state, V_N, using classical equations of motion.[47-50] To first order, the evolution of the wavepacket is thus dictated by the gradient of the upper state potential with respect to the vibrational coordinate of the lower electronic state, which increases with greater displacement of the equilibrium geometry of V_N.

$$I_k \propto \omega_p(\omega_p - \omega_k)^3 \left|\alpha_{fi}^k\right|^2 \approx \omega_p(\omega_p - \omega_k)^3 \frac{|\mu_{NI}|^4}{2\omega_k}\left(\frac{\partial V_N}{\partial q_k}\right)^2,$$

where ω_k is the mode frequency, q_k is the normalised mode coordinate, ω_p is the excitation (pump) frequency and μ_{NI} is the electric transition dipole moment between the lower and upper electronic state.[45] The resonance Raman intensity is therefore also strongly dependent on the oscillator strength of the electronic transition, $f \propto E_p|\mu_{NI}|^2$ where $E_p = \hbar\omega_p$.[44]

The Condon approximation for the electric transition dipole moment restricts the gradient approximation to the Albrecht A term in the theory of Raman scattering, neglecting any Herzberg-Teller vibronic coupling between electronic states involved in the higher (B, C, D) terms.[51] These terms are expected to have a greater contribution in excited state resonance Raman spectra, where the increased density of states reduces the separation energies. In this format, the gradient approximation is limited to resonance with a single electronic state, neglecting any mode enhancement due to the additive effects of resonance with nearby excited states. Similarly, this approach does not account for quantum interference caused by allowed transitions to multiple electronic states or population transfer due to nonadiabatic coupling between states, which result in resonance de-enhancement.[52-53] Reduced enhancement due to homogeneous broadening, most significant for low frequency modes, is also neglected in this approach.[45, 54-55]

Methods

(i) Femtosecond Stimulated Raman The experimental FSRS spectra we aim to simulate were measured previously[41] using an instrument described in detail elsewhere.[56-57] The narrowband (ca. 10 cm^{-1}) picosecond 'Raman Pump' pulses was centered at 750 nm to be resonant with the known excited state transient absorption of FAD.[40] The excitation was at 450 nm, generated from the OPA (Topas Prime).

(ii) Off-resonance Raman Calculations. The optimized structures and off-resonance Raman spectra were calculated as described in our previous paper (see also supporting information).[41] All calculations were completed using Gaussian 16.[58] The ribityl-5'-phosphate in FMN was replaced with a methyl

group for most calculations, thus modelling the isoalloxazine chromophore in FMN as lumiflavin. The lumiflavin was solvated by four explicit water molecules[38] as well as a polarizable continuum model (PCM)[59-60] for water. The optimized structure of the ground electronic state, S_0, was obtained using DFT at the B3LYP[61-62]/TZVP[63] level of theory and is presented in figure 1, showing the arrangement of water molecules around the polar end of isoalloxazine. This level of theory was chosen to align with our earlier work and previous studies,[38,41] in addition to the functional being well established and benchmarked for frequency calculations. The four water molecules represent the H-bonding interaction, which causes a red-shift of ππ* and a blue-shift of nπ* transitions such that $S_0 \rightarrow S_1$ corresponds to an allowed ππ* transition.[38, 64-65] The orientation of the water molecules lowers the symmetry from the C_S to C_1 point group. The excited state geometries were optimized using TD-DFT for S_1 and unrestricted DFT for T_1 at the same level of theory and solvation used for the ground state. The three optimized structures were characterised using harmonic frequency analysis at 298.15 K and 1 atm, identifying genuine minima and yielding off-resonance Raman spectra for each of S_0, S_1, and T_1.

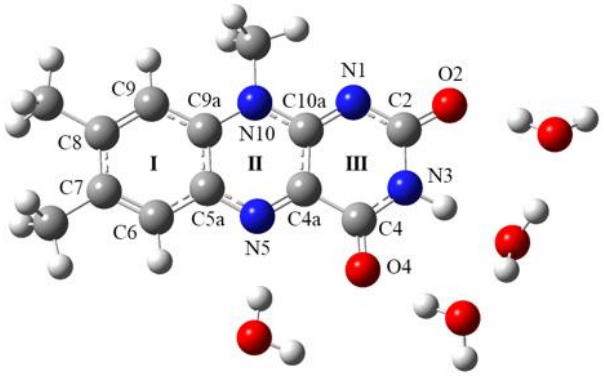

Figure 1*: Optimized geometry of lumiflavin in the ground electronic state (S_0) with atomic labels, obtained using B3LYP/TZVP level of theory solvated by four water molecules as well as a PCM.*

(iii) Resonance Raman Calculations. Resonance Raman spectra for each of S_0, S_1, and T_1 are calculated using the gradient approximation method as described for FSRS by Elles *et al.*[44-45] TD-DFT calculations are repeated for several steps along each vibrational mode coordinate of the lower state, S_i or T_i, including the optimised geometry, providing the potential energy surfaces of the upper excited states, S_N or T_N, in this region. The potential energy surfaces are then fit with a polynomial function and differentiated to evaluate the gradients of the upper states at the optimised geometry of the lower

state, as required for equation 1. Here, TD-DFT was performed for five steps along the normalized mode coordinate, $q_k = 0, \pm 0.1, \pm 0.2$, for all modes in the range 1150 - 1750 cm^{-1} (31 modes for each of the ground excited singlet and triplet states) and the resulting potential energy surfaces were accurately fit with a cubic function to account for the anharmonicity implicit to TD-DFT (see supporting information). The appropriate upper excited state to be used in equation 1 corresponds to the transition approaching resonance with the excitation wavelength which has the greatest oscillator strength, as discussed below. Transition dipole moments between excited singlet states are obtained from the TD-DFT results at the optimized geometry of S_1 using the Multiwfn program.[66]

As discussed by Elles *et al.*, this method is limited by the inability of TD-DFT to account for double-excitation character of electronic states, which may be overcome by using alternative methods such as equation-of-motion coupled-cluster theory with single and double excitations (EOM-CCSD).[44] Significant double-excitation character is expected for higher excited states populated by the sequential absorption of two photons, such as the resonant singlet states, S_N. However, the rapid scaling in computational cost with increasing system size for coupled-cluster methods warrants less demanding TD-DFT for studies involving repeated calculation for larger molecules, such as lumiflavin.[67-69]

Results and Discussion

In our previous paper, transitions in the FSRS spectra of the S_1 and T_1 excited states of FMN were assigned through comparison of the shifts observed for a series of isotopologues with shifts in the calculated off-resonance Raman spectra. However, as off-resonance spectra neglect the enhancement due to the gradient of the resonant state involved in FSRS, the assignments were based primarily on the calculated mode frequencies, and the observed peaks are often associated with several calculated modes. The transient absorption spectra of FMN at early times show a broad $S_1 \rightarrow S_n$ excited state absorption band from ca. 700 - 900 nm which probably involves multiple excited singlet states. At later times a more intense $T_1 \rightarrow T_n$ band is observed at 712 nm, which is pre-resonant with the 750 nm

excitation wavelength, leading to significant resonance enhancement.[40] Calculation of the resonance Raman spectra using the gradient approximation method described above should therefore enable an improved assignment of the S_1 and T_1 FSRS peaks, by accounting for the enhancement due to the resonant singlet and triplet states. First, the model is benchmarked against the well-known resonance Raman spectrum for the ground electronic state (S_0) of isoalloxazine, and then applied to calculate resonance Raman spectra for the excited states S_1 and T_1, which are then used to refine the assignment of the measured FSRS peaks.

(i) S_0 Benchmark. Calculated off-resonance and resonance Raman spectra for the ground state, S_0, are presented in figure 2. The calculated frequencies for S_0 include an empirical scaling factor of 0.965 commonly used for this level of theory and basis set.[70] The ground state resonance Raman spectra reported for both riboflavin[42-43] and lumiflavin[71] show excellent agreement with the calculated spectrum. The resonance Raman spectrum of riboflavin reported by Kitagawa *et al.* identifies five strongly enhanced modes at 1252, 1355, 1407, 1584 and 1631 cm^{-1},[42] which correspond to transitions at 1204, 1312, 1543 and 1605 cm^{-1} in the calculated spectrum. However, no enhancement was calculated at 1407 cm^{-1} while a calculated enhancement at 1502 cm^{-1} has no experimental counterpart. The missing enhancement at 1407 cm^{-1} is similarly weak when calculated using the independent mode, displaced harmonic oscillator (IMDHO) model, as reported by Weigel *et al.*[38]and Kar *et al.*[71] IMDHO uses the same time-dependent theory as the semiclassical gradient approximation described above, but assumes the excited state potential energy surfaces are harmonic.[72]

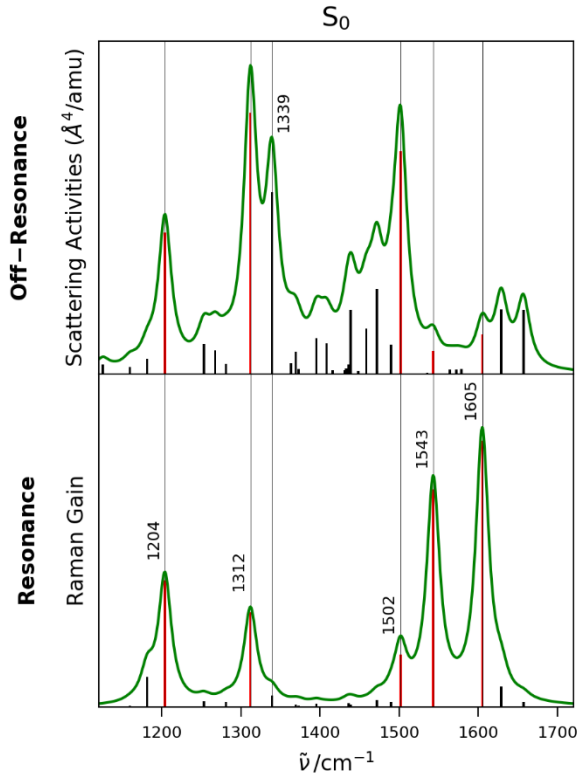

***Figure 2**: Calculated off-Resonance and Resonance Raman spectra for S_0 of lumiflavin solvated by four water molecules. Resonance enhanced modes are highlighted in red.*

The resonance Raman spectrum in figure 2 is calculated using the gradient of the S_1 potential energy surface at the optimised geometry of S_0, with an excitation wavelength of 488 nm to match the literature. The calculated spectra are broadened by a Lorentzian function with FWHM of 20 cm^{-1} and scaled so that the original 'stick' spectra are contained within the lineshape. The five modes with the strongest enhancement in the resonance Raman spectrum are assigned in Table 1 and highlighted in red in Figure 2. Modes are numbered according to the output of the frequency analysis at the optimised geometry for each electronic state. The numbering of modes for S_0 in Table 1 is therefore independent of the numbering for S_1 and T_1 modes discussed later. The assignment of these modes agrees with that of Weigel *et al.* using the IMDHO model, as well as the displacements identified through isotopic frequency shifts by Kitigawa *et al.*[38, 42]

Experimental[42] /cm^{-1}	Calculated /cm^{-1}	Mode	Assignment
1252	1204	75	*as*C2-N3-C4, *s*C7-Me, *s*C8-Me, *w*C6-H, *w*C9-H
1355	1312	79	*as*N10-C10a-C4a, *ss*C2-N3-C4, *as*C5a-C9a-C9, *s*C7-C8, *w*C6-H
-	1502	95	*as*N10-C10a-N1, *s*C4a-N5, *ss*C8-C9-C9a, *ss*(C2=O2, C4=O4), *w*N3-H, *b*N10-Me
1584	1543	97	*s*C5a-C9a, *as*C7-C8-C9, *as*N5-C4a-C10a
1631	1605	101	*s*C4a-N5, *s*C6-C7, *s*C9-C9a, *s*C2=O2

Table 1*: Assignment of resonance enhanced modes for S_0. s: stretch, a-: antisymmetric, s-: symmetric, w: wag, b: bend. Three atom stretches are described with respect to the centre atom and delocalised/coupled carbonyl stretches are indicated using brackets.*

The resonance enhanced modes at 1204 cm^{-1}, 1312 cm^{-1} and 1502 cm^{-1} also produce intense peaks in the off-resonance Raman spectrum, in contrast to the most enhanced modes at 1543 cm^{-1} and 1605 cm^{-1}. The intense peak in the off-resonance Raman spectrum at 1339 cm^{-1} shows minimal enhancement in the resonance Raman spectrum. The carbonyl stretches at 1629 cm^{-1} and 1657 cm^{-1} also show very little enhancement in the resonance Raman spectrum, reflecting the negligible displacement between the potential minima for S_1 and S_0 for these modes. All five modes in Table 1 feature strong C-N as well as ring I stretches such that the vibrations are delocalised across the isoalloxazine moiety.

(ii) S_1 Assignment. The calculated off-resonance and resonance Raman spectra for S_1 are shown in figure 3. The modes with the greatest resonance enhancement are again highlighted in red to emphasise the contrast with off-resonance intensities. The previously reported[41] FSRS spectrum for S_1 is also shown in figure 3. Recognizing the dominance of the transition dipole moment in equation 1, $\propto |\mu_{NI}|^4$, the resonance Raman spectrum is calculated using the gradient of S_8 for the upper state, as the TD-DFT results identify $S_1 \rightarrow S_8$ has the greatest oscillator strength of transitions in the region of the 750 nm Raman pump wavelength. The energies and oscillator strengths of neighbouring transitions are provided in the supplementary information. The assignment of each peak in the FSRS spectrum of S_1 is given in table 2, including the modes identified in our previous work using isotopic frequency shifts in off-resonance spectra, as well as the refinements now proposed by the calculated resonance Raman spectrum.

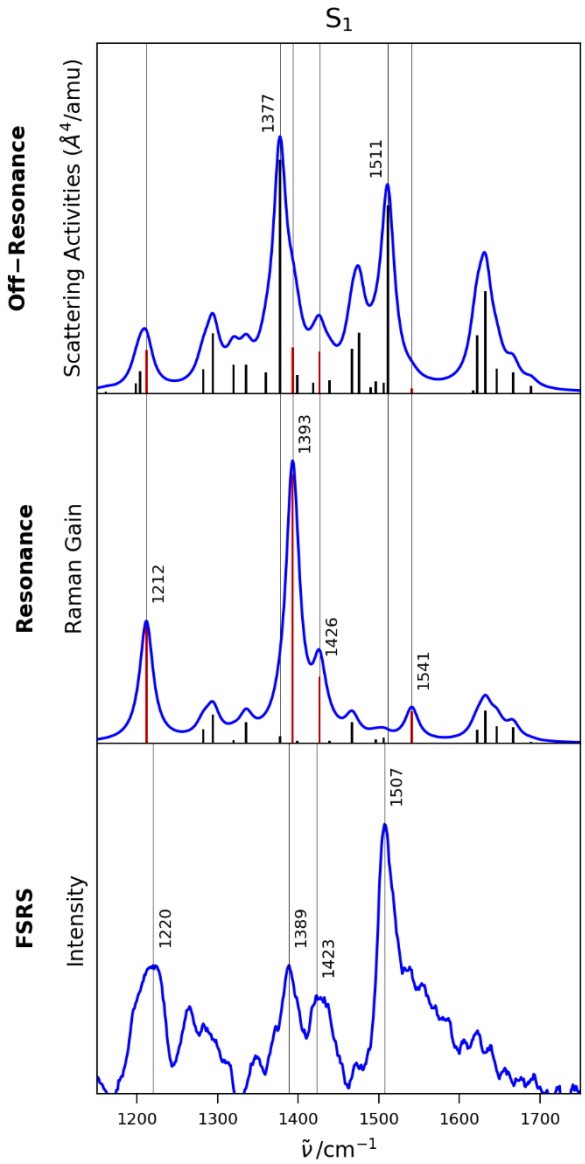

***Figure 3**: Calculated off-Resonance and Resonance Raman spectra for S_1 of lumiflavin solvated by four water molecules, as well as measured FSRS spectrum for S_1 of FMN in H_2O from ref[41]. Resonance enhanced modes are highlighted in red.*

FSRS /cm^{-1}	Off-Resonance Raman /cm^{-1}	Resonance Raman /cm^{-1}	Mode	Assignment
1220	1198		73	*s*N5-C5a, *s*N3-C4, *s*C6-C7, *w*C6-H, *w*C9-H
	1204		74	*s*C2-N3, *ss*N5-C4a-C10a, *s*C9-C9a, *s*C6-C7, *w*C6-H, *w*C9-H, *w*N10-Me
	1212	1212	75	*as*C10a-N1-C2, *s*N3-C4, *s*C4a-N5, *s*C6-C7
1389	1360		80	*s*N10-C10a, *s*N3-C4, *as*C7-C8-C9, *as*C6-C5a-C9a, *b*N10-Me, *b*C7-Me, *b*C8-Me
	1377		81	*s*C4a-C10a, *s*N1-C2, *s*C5a-C9a, *s*C6-C7, *w*C6-H
	1393	1393	82	*s*C4a-N5, *s*N10-C10a, *s*N1-C2, *ss*C8-C9-C9a, *w*C6-H, *b*N10-Me, *w*C8-Me, *w*C7-Me
1423	1426	1426	85	*as*N5-C4a-C4, *ss*C10a-N1-C2, *s*N3-C4, *w*C6-H, *sc*C8-Me, *sc*N10-Me
1507	1511		95	*s*C4a-N5, *s*N1-C10a, *s*C7-C8, *s*C5a-C9a, *w*N3-H, *b*C7-Me, *b*C8-Me, *b*N10-Me, *w*C9-H, *w*C6-H

***Table 2**: Assignment of FSRS peaks for S_1 based on the calculated off-resonance and resonance Raman spectra. s: stretch, a-: antisymmetric, s-: symmetric, w: wag, sc: scissor, b: bend. Three atom stretches are described with respect to the centre atom.*

The off-resonance Raman spectrum associates the FSRS peak at 1220 cm^{-1} with a cluster of ring modes 73, 74 and 75. The isolated enhancement of mode 75 at 1212 cm^{-1} in the resonance Raman spectrum now refines this assignment. Similarly, ^{15}N or ^{13}C substitution resulted in a red-shift of the FSRS peak at 1389 cm^{-1} which was also shown by modes 80, 81 and 82, where mode 81 at 1377 cm^{-1} has the greatest intensity in the off-resonance spectrum, but mode 82 best reproduced the red-shifts of the FSRS peak. The resonance Raman spectrum shows negligible enhancement of mode 81, in favour of significant enhancement of mode 82 at 1393 cm^{-1}. The 1389 cm^{-1} peak is therefore assigned to mode 82 which features strong C-N and ring I stretches, as observed for the enhanced ground state vibrations, whereas the greatest displacements involved in mode 81 are localised on ring II; calculated mode displacements are shown in the supplementary information. The resonance Raman spectrum confirms the assignment of the FSRS peak at 1423 cm^{-1} to mode 85 at 1426 cm^{-1}. However, the FSRS peak at 1507 cm^{-1} has no clear assignment in the calculated resonance Raman spectrum. The peak at 1507 cm^{-1} shows twice the amplitude of the other FSRS peaks and was insensitive to ^{15}N or ^{13}C

substitution and D_2O exchange. Despite the intensity of mode 95 at 1511 cm^{-1} in the off-resonance spectrum, this mode shows no enhancement in the resonance Raman spectrum. Similarly, the small enhancement of mode 96 at 1541 cm^{-1} does not account for the dominance of the 1507 cm^{-1} peak in the FSRS spectrum, though it may contribute to the shoulder to higher wavenumber of the peak (figure 3).

The difficulties in assigning the 1507 cm^{-1} peak must therefore result from the limitations of the gradient approximation, which does not account for vibronic coupling between electronic states, or the density of excited states. The neglect of vibronic coupling means that overtones and combination bands are not resolved in the resonance Raman spectra calculated using this method. The absence of a fundamental mode enhancement at ca. 1500 cm^{-1} therefore suggests consideration of a possible assignment of the 1507 cm^{-1} FSRS peak to an overtone or combination of lower frequency modes. In the limit of strong damping, typical for large molecules in the condensed phase, the intensities of overtones and combination bands are also determined by the displacement of the upper state potential energy surface, but cannot exceed the intensities of the fundamental peaks for the contributing modes.[46, 73] This was demonstrated by Quincy *et al.* for a combination band of diphenylthiophene, where the fundamental peaks of the contributing modes are clearly visible at lower frequency in the FSRS spectrum, and are significantly (> 6 times) more intense.[44] However, extension of the calculated resonance Raman spectra for S_1 isoalloxazine to the lower frequency 400 - 900 cm^{-1} region identified no modes that exceeded, or even matched, the intensity of the peaks in figure 3. Thus an assignment to an overtone or combination band is not supported.

Strong peaks at ca. 1500 cm^{-1} were also observed in the FSRS spectra of S_1 reported by Weigel *et al.* and Andrikopoulos *et al.*, and assigned using off-resonance calculations.[38, 40] However, Andrikopoulos *et al.* reported that the assignment of this strong peak had the greatest difference between calculated and experimental frequencies; these complications are consistent with the present difficulties.[40] If the peak at 1507 cm^{-1} is indeed the result of a separate vibrational mode, the missing enhancement must also reflect the limitations of TD-DFT in describing the higher excited singlet states.

Another possibility is a role for a different enhancing transition, although the order of magnitude decrease in oscillator strength for transitions to states neighbouring S_8 suggests the density of electronic states is not the primary issue (supporting information). Even so this possibility was investigated. There is also no strong enhancement at ca. 1500 cm^{-1} in resonance Raman spectra calculated using S_6 and S_7 as alternative near resonant states, so this is also not a plausible explanation (supporting information).

(iii) T_1 Assignment. The calculated off-resonance and resonance Raman spectra for T_1 are shown in figure 4, along with the previously reported FSRS spectrum of T_1 recorded 3 ns after electronic excitation to allow for intersystem crossing.[41] The resonance Raman spectrum is calculated using the gradient of T_5 for the upper state, selected as the oscillator strength of the $T_1 \rightarrow T_5$ transition is two orders of magnitude greater than $T_1 \rightarrow T_4$, although the transition energy is further from resonance with the 750 nm Raman pump wavelength; see supplementary information. This is in line with the dominant role of transition dipole moment in the enhancement. Assignments of the FSRS peaks for T_1 are given in table 3.

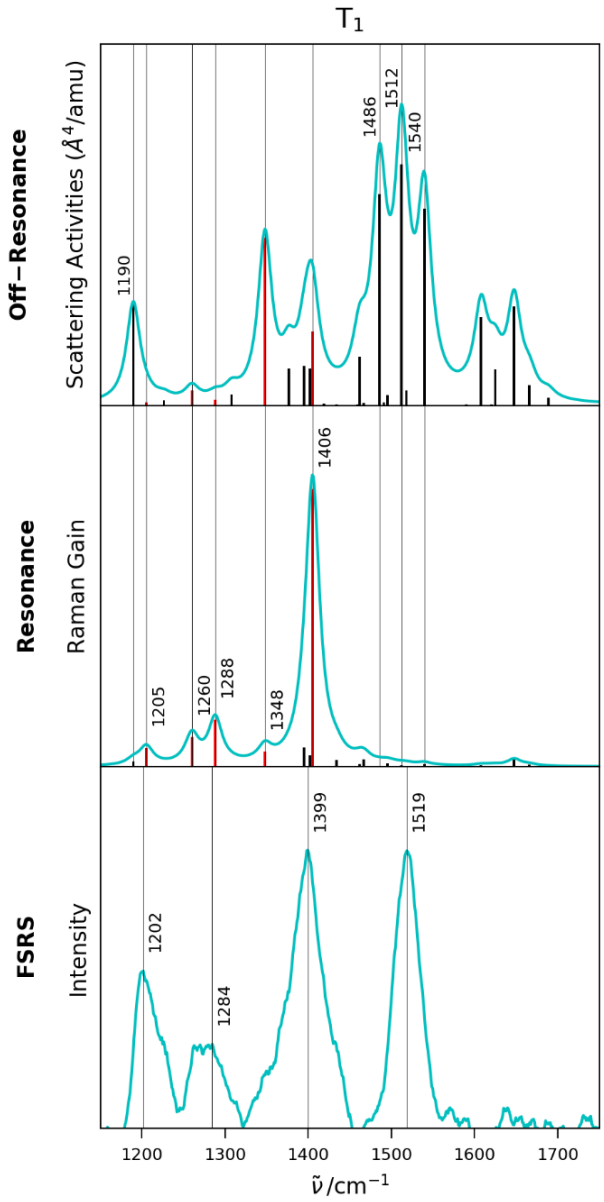

***Figure 4**: Calculated off-Resonance and Resonance Raman spectra for T_1 of lumiflavin solvated by four water molecules, as well as measured FSRS spectrum for T_1 of FMN in H_2O from ref. [41] Resonance enhanced modes are highlighted in red.*

FSRS /cm^{-1}	Off-Resonance Raman /cm^{-1}	Resonance Raman /cm^{-1}	Mode	Assignment
1202	1190		73	*as*N1-C2-N3, *as*C4-C4a-C10a, *as*C5a-C6-C7, *w*C6-H, *ss*C8-C9-C9a
		1205	74	*s*N3-C4, *s*C5a-N5, *s*C9-C9a, *w*C6-H, *w*C9-H, *w*N10-Me
1284	1260	1260	76	*as*C2-N3-C4, *s*N10-C10a, *s*C4a-N5, *s*C6-C7, *w*C6-H, *w*N10-Me
		1288	77	*s*C7-Me, *s*C5a-N5, *s*N10-Me, *s*N1-C2, *w*C6-H, *w*C9-H
1399	1348		79	*s*N10-Me, *s*N1-C10a, *ss*C2-N3-C4, *as*C6-C7-C8, *as*C9-C9a-C5a, *w*C6-H, *w*C9-H
	1395		81	*s*N1-C10a, *s*C4a-N5, *ss*C2-N3-C4, *s*C9-C9a, *b*C7-Me, *w*N3-H
	1406	1406	83	*s*N10-C10a, *s*C4a-N5, *s*N1-C2, *s*N3-C4, *ss*C8-C9-C9a, *w*C7-Me, *w*C8-Me, *w*N10-Me
1519	1486		90	*s*C4a-N5, *s*N1-C10a, *as*(C2=O2, C4=O4), *w*N3-H
	1512		94	*s*C4a-N5, *s*N1-C10a, *ss*C5a-C6-C7, *s*C8-Me, *s*C9a-N10, *w*N3-H, *b*N10-Me, *b*C7-Me
	1540		96	*s*C4a-N5, *s*N1-C10a, *s*C2=O2, *s*N3-C4, *ss*C7-C8-C9, *w*C6-H, *w*C9-H, *w*N3-H

Table 3*: Assignment of FSRS peaks for T_1 based on the calculated off-resonance and resonance Raman spectra. s: stretch, a-: antisymmetric, s-: symmetric, w: wag, b: bend. Three atom stretches are described with respect to the centre atom and delocalised/coupled carbonyl stretches are indicated using brackets.*

The off-resonance Raman spectrum identified mode 73 at 1190 cm^{-1} as the only candidate for the FSRS peak at 1202 cm^{-1}, but the resonance Raman spectrum shows this mode has negligible enhancement so this peak is in fact better assigned to mode 74 at 1205 cm^{-1}, which has the greater amplitude in the resonance spectrum. Again, mode 74 is delocalised across the isoalloxazine structure whereas mode 73 has the strongest amplitude displacements concentrated on ring III. The resonance Raman spectrum confirms the earlier assignment of the FSRS peak at 1284 cm^{-1} to modes 76 and 77 at 1260 cm^{-1} and 1288 cm^{-1}, respectively, which have minimal intensity in the off-resonance spectrum, but moderate enhancement in the resonance Raman spectrum. The resonance Raman spectrum for T_1 is dominated by enhancement of mode 83 at 1406 cm^{-1}. The FSRS peak at 1399 cm^{-1} can therefore be confidently assigned to mode 83, whereas the isotopic frequency shifts in the off-resonance Raman

spectra had previously not distinguished between modes 79, 81 or 83 as possible assignments. As was found for S_1, the lack of enhancement in the region of 1500 cm^{-1} means assignment of the FSRS peak at 1519 cm^{-1} cannot be improved beyond the previous suggestions of modes 90, 94 and 96 from the off-resonance Raman spectrum; none of these modes are strongly enhanced. This dramatic difference in intensity between the off-resonance and resonance Raman spectra for both S_1 and T_1 demonstrates that assignments based purely on off-resonance spectra may be unreliable.

The 1519 cm^{-1} peak showed no significant change on D_2O exchange, with modes 90 and 96 both reproducing the red-shift of the FSRS peak on ^{15}N and ^{13}C substitution, but again the absence of an enhancement places a question mark over this assignment. Extension of the calculated resonance Raman spectrum to the lower frequency 400 - 900 cm^{-1} region again did not identify any modes with sufficient enhancements to support assignment of the 1519 cm^{-1} peak to an overtone or combination band. Therefore, the missing enhancement of this peak links with the 1507 cm^{-1} FSRS peak for S_1, suggesting a common origin and thus endorsing the blue-shift of this mode on triplet formation, as described previously by both us and Andrikopoulos *et al.*[40] Resonance Raman spectra calculated using T_4 or T_6 as the resonant state show increased enhancement above 1500 cm^{-1}, including the carbonyl stretching modes, but any contribution from these states is expected to be negligible due to the significantly reduced oscillator strength; see supplementary information.

One final possible assignment for the missing 1507/1519 cm^{-1} bands is that our simulations are based on isoalloxazine, whereas measurements were made on FMN, so potentially the side chain might make a contribution. This is unexpected, as the most strongly enhanced modes are delocalized ring modes, but as a check we extended the TDDFT calculation to riboflavin, which has the same side chain as FMN, but does not include the phosphate group. Although some differences were found in the electronic structure and the off-resonance spectrum between isoalloxazine and FMN, the overall pattern of the enhancements was not modified, and in particular there were no new candidates for the identity of the 1507/1519 cm^{-1} bands; these data are presented in the supporting information. The

absence of these experimentally observed modes in the calculated enhancements therefore suggests some shortcoming in the methods employed here.

Conclusions

Resonance enhanced FSRS provides a powerful means of studying the structure of excited electronic states of large molecules in complex environments. It provides data beyond anything that can be gleaned from transient absorption spectroscopy. The method has recently been applied to investigate the isoalloxazine moiety in solution and in photoactive flavoproteins. These studies have been supported by TD-DFT calculations, but assignment of FSRS peaks based on off-resonance Raman spectra is challenging because of the large number of modes, and neglects the essential contribution of the resonant excited state in determining the intensities. Here, the assignment of FSRS spectra for S_1 and T_1 states of FMN, previously reported by a number of groups, has been addressed through calculation of excited state resonance Raman spectra, using the time-dependent gradient approximation. The calculated resonance Raman spectra have confirmed or refined the assignment of almost all FSRS peaks observed for FMN or riboflavin. The generally good agreement between experiment and the time-dependent gradient approximation is encouraging. However, for both S_1 and T_1 FMN a prominent band at ca. 1500 cm^{-1} in the FSRS spectrum was absent from the calculations. This may be due to the neglect of Herzberg-Teller vibronic couplings within the gradient approximation, or may also reflect the inadequacy of TD-DFT to correctly characterise the higher energy, resonant excited electronic S_n/T_n states. Employing alternative excited state methods such as EOM-CCSD to obtain the excited state potential energy surfaces might reduce these concerns and so identify the missing mode. Furthermore, the use of a post Hartree-Fock methodology, such as MP2, would account for correlation energies more accurately and therefore give a better description of the molecular geometries, especially with regards to the positioning of the explicit solvent molecules. Using MP2 for geometric optimizations in combination with EOM-CCSD for excited state calculations

should be considered for future studies, this will however be at considerable (perhaps prohibitive) additional computational expense.

Acknowledgements

This study was supported by the National Science Foundation (NSF) (MCB-1817837 to PJT) and the EPSRC (EP/N033647/1 EP/R042357/1, EP/J009148/1 to SRM). JNI was supported by a National Institutes of Health Chemistry-Biology Interface Training Grant (T32GM092714). AL acknowledges funding from EFOP-3.6.2-16-2017-00005. Calculations presented in this paper were carried out on the High Performance Computing Cluster supported by the Research and Specialist Computing Support service at the University of East Anglia.

Supporting information. The supporting information describes the calculated optimized geometries, excited state transition energies and oscillator strengths, the resonance Raman potential energy surface fitting to calculate enhancements, additional resonance Raman spectra and key vibrational mode displacements. In addition, the extension to riboflavin FMN calculations is described.

REFERENCES

1. Massey, V., The Chemical and Biological Versatility of Riboflavin. *Biochem. Soc. Trans.* **2000**, *28*, 283-296.
2. Losi, A.; Gartner, W., The Evolution of Flavin-Binding Photoreceptors: An Ancient Chromophore Serving Trendy Blue-Light Sensors. In *Annu. Rev. Plant Biol., Vol 63*, Merchant, S. S., Ed. 2012; Vol. 63, pp 49-72.
3. Losi, A.; Gartner, W., Old Chromophores, New Photoactivation Paradigms, Trendy Applications: Flavins in Blue Light-Sensing Photoreceptors. *Photochem. Photobiol.* **2010**, *87*, 491-510.
4. Masuda, S., Light Detection and Signal Transduction in the Bluf Photoreceptors. *Plant Cell Physiol.* **2013**, *54*, 171-179.
5. Crosson, S.; Rajagopal, S.; Moffat, K., The Lov Domain Family: Photoresponsive Signaling Modules Coupled to Diverse Output Domains†. *Biochemistry* **2002**, *42*, 2-10.
6. Christie, J. M.; Swartz, T. E.; Bogomolni, R. A.; Briggs, W. R., Phototropin Lov Domains Exhibit Distinct Roles in Regulating Photoreceptor Function. *Plant J.* **2002**, *32*, 205-219.
7. Kottke, T.; Hegemann, P.; Dick, B.; Heberle, J., The Photochemistry of the Light-, Oxygen-, and Voltage-Sensitive Domains in the Algal Blue Light Receptor Phot. *Biopolymers* **2006**, *82*, 373-378.
8. Sancar, A., Structure and Function of DNA Photolyase and Cryptochrome Blue-Light Photoreceptors. *Chem. Rev.* **2003**, *103*, 2203-2237.
9. Losi, A.; Gardner, K. H.; Moglich, A., Blue-Light Receptors for Optogenetics. *Chem. Rev.* **2018**, *118*, 10659-10709.
10. Kandori, H., Structure/Function Study of Photoreceptive Proteins by Ftir Spectroscopy. *Bull. Chem. Soc. Jpn* **2020**, *93*, 904-926.
11. Massey, V.; Hemmerich, P., Photoreduction of Flavoproteins and Other Biological Compounds Catalyzed by De-Aza-Flavins. *Biochemistry* **1978**, *17*, 9-16.
12. Abe, M.; Kyogoku, Y.; Kitagawa, T.; Kawano, K.; Ohishi, N.; Takaisuzuki, A.; Yagi, K., Infrared-Spectra and Molecular Association of Lumiflavin and Riboflavin Derivatives. *Spectrochim. Acta A Mol. Biomol. Spectrosc.* **1986**, *42*, 1059-1068.
13. Unno, M.; Sano, R.; Masuda, S.; Ono, T. A.; Yamauchi, S., Light-Induced Structural Changes in the Active Site of the Bluf Domain in Appa by Raman Spectroscopy. *J. Phys. Chem. B* **2005**, *109*, 12620-12626.
14. Winkler, A.; Heintz, U.; Lindner, R.; Reinstein, J.; Shoeman, R. L.; Schlichting, I., A Ternary Appa–Ppsr–DNA Complex Mediates Light Regulation of Photosynthesis-Related Gene Expression. *Nat. Struct. Mol. Biol.* **2013**, *20*, 859-867.
15. Jung, A.; Reinstein, J.; Domratcheva, T.; Shoeman, R. L.; Schlichting, I., Crystal Structures of the Appa Bluf Domain Photoreceptor Provide Insights into Blue Light-Mediated Signal Transduction. *J. Mol. Biol.* **2006**, *362*, 717-732.
16. Jung, A.; Domratcheva, T.; Tarutina, M.; Wu, Q.; Ko, W. H.; Shoeman, R. L.; Gomelsky, M.; Gardner, K. H.; Schlichting, L., Structure of a Bacterial Bluf Photoreceptor: Insights into Blue Light-Mediated Signal Transduction. *Proc. Natl. Acad. Sci. U. S. A.* **2005**, *102*, 12350-12355.
17. Harper, S. M.; Christie, J. M.; Gardner, K. H., Disruption of the Lov-J Alpha Helix Interaction Activates Phototropin Kinase Activity. *Biochemistry* **2004**, *43*, 16184-16192.
18. Harper, S. M.; Neil, L. C.; Gardner, K. H., Structural Basis of a Phototropin Light Switch. *Science* **2003**, *301*, 1541-1544.
19. Lukacs, A.; Eker, A. P. M.; Byrdin, M.; Brettel, K.; Vos, M. H., Electron Hopping through the 15 Angstrom Triple Tryptophan Molecular Wire in DNA Photolyase Occurs within 30 Ps. *J. Am. Chem. Soc.* **2008**, *130*, 14394-+.
20. Gauden, M.; van Stokkum, I. H. M.; Key, J. M.; Luhrs, D. C.; Van Grondelle, R.; Hegemann, P.; Kennis, J. T. M., Hydrogen-Bond Switching through a Radical Pair Mechanism in a Flavin-Binding Photoreceptor. *Proc. Natl. Acad. Sci. U. S. A.* **2006**, *103*, 10895-10900.

21. Kennis, J. T. M.; Crosson, S.; Gauden, M.; van Stokkum, I. H. M.; Moffat, K.; van Grondelle, R., Primary Reactions of the Lov2 Domain of Phototropin, a Plant Blue-Light Photoreceptor. *Biochemistry* **2003**, *42*, 3385-3392.
22. Kao, Y. T.; Saxena, C.; He, T. F.; Guo, L. J.; Wang, L. J.; Sancar, A.; Zhong, D. P., Ultrafast Dynamics of Flavins in Five Redox States. *J. Am. Chem. Soc.* **2008**, *130*, 13132-13139.
23. Goings, J. J.; Li, P. F.; Zhu, Q. W.; Hammes-Schiffer, S., Formation of an Unusual Glutamine Tautomer in a Blue Light Using Flavin Photocycle Characterizes the Light-Adapted State. *Proc. Natl. Acad. Sci. U. S. A.* **2020**, *117*, 26626-26632.
24. Goyal, P.; Hammes-Schiffer, S., Role of Active Site Conformational Changes in Photocycle Activation of the Appa Bluf Photoreceptor. *Proc. Natl. Acad. Sci. U. S. A.* **2017**, *114*, 1480-1485.
25. Domratcheva, T.; Hartmann, E.; Schlichting, I.; Kottke, T., Evidence for Tautomerisation of Glutamine in Bluf Blue Light Receptors by Vibrational Spectroscopy and Computational Chemistry. *Scientific Reports* **2016**, *6*.
26. Udvarhelyi, A.; Domratcheva, T., Glutamine Rotamers in Bluf Photoreceptors: A Mechanistic Reappraisal. *J. Phys. Chem. B* **2013**, *117*, 2888-2897.
27. Dittrich, M.; Freddolino, P. L.; Schulten, K., When Light Falls in Lov: A Quantum Mechanical/Molecular Mechanical Study of Photoexcitation in Phot-Lov1 of Chlamydomonas Reinhardtii. *J. Phys. Chem. B* **2005**, *109*, 13006-13013.
28. Konold, P. E.; Mathes, T.; Weiβenborn, J.; Groot, M. L.; Hegemann, P.; Kennis, J. T. M., Unfolding of the C-Terminal Jα Helix in the Lov2 Photoreceptor Domain Observed by Time-Resolved Vibrational Spectroscopy. *J. Phys. Chem. Letters* **2016**, 3472-3476.
29. Alexandre, M. T. A.; Domratcheva, T.; Bonetti, C.; van Wilderen, L. J. G. W.; van Grondelle, R.; Groot, M.-L.; Hellingwerf, K. J.; Kennis, J. T. M., Primary Reactions of the Lov2 Domain of Phototropin Studied with Ultrafast Mid-Infrared Spectroscopy and Quantum Chemistry. *Biophys. J.* **2009**, *97*, 227-237.
30. Alexandre, M. T. A.; van Wilderen, L. J. G.; van Grondelle, R.; Hellingwerf, K. J.; Groot, M. L.; Kennis, J. T. M., Early Steps in Blue Light Reception by Plants: An Ultrafast Mid-Infrared Spectroscopic Study of the Lov2 Domain of Phototropin. *Biophys. J.* **2005**, *88*, 509A-509A.
31. Iuliano, J. N., et al., Variation in Lov Photoreceptor Activation Dynamics Probed by Time-Resolved Infrared Spectroscopy. *Biochemistry* **2017**.
32. Gil, A. A., et al., Photoactivation of the Bluf Protein Pixd Probed by the Site-Specific Incorporation of Fluorotyrosine Residues. *J. Am. Chem. Soc.* **2017**, *139*, 14638-14648.
33. Lukacs, A.; Haigney, A.; Brust, R.; Zhao, R. K.; Stelling, A. L.; Clark, I. P.; Towrie, M.; Greetham, G. M.; Meech, S. R.; Tonge, P. J., Photoexcitation of the Blue Light Using Fad Photoreceptor Appa Results in Ultrafast Changes to the Protein Matrix. *J. Am. Chem. Soc.* **2011**, *133*, 16893-16900.
34. Stelling, A. L.; Ronayne, K. L.; Nappa, J.; Tonge, P. J.; Meech, S. R., Ultrafast Structural Dynamics in Bluf Domains: Transient Infrared Spectroscopy of Appa and Its Mutants. *J. Am. Chem. Soc.* **2007**, *129*, 15556-15564.
35. Lorenz-Fonfria, V. A., Infrared Difference Spectroscopy of Proteins: From Bands to Bonds. *Chem. Rev.* **2020**, *120*, 3466-3576.
36. Frontiera, R. R.; Mathies, R. A., Femtosecond Stimulated Raman Spectroscopy. *Laser Photonics Rev.* **2011**, *5*, 102-113.
37. Kukura, P.; McCamant, D. W.; Mathies, R. A., Femtosecond Stimulated Raman Spectroscopy. In *Annu. Rev. Phys. Chem.*, 2007; Vol. 58, pp 461-488.
38. Weigel, A.; Dobryakov, A.; Klaumunzer, B.; Sajadi, M.; Saalfrank, P.; Ernsting, N. P., Femtosecond Stimulated Raman Spectroscopy of Flavin after Optical Excitation. *J. Phys. Chem. B* **2011**, *115*, 3656-3680.
39. Hall, C. R.; Heisler, I. A.; Jones, G. A.; Frost, J. E.; Gil, A. A.; Tonge, P. J.; Meech, S. R., Femtosecond Stimulated Raman Study of the Photoactive Flavoprotein Appa(Bluf). *Chem. Phys. Lett.* **2017**, *683*, 365-369.

40. Andrikopoulos, P. C., et al., Femtosecond-to-Nanosecond Dynamics of Flavin Mononucleotide Monitored by Stimulated Raman Spectroscopy and Simulations. *Phys. Chem. Chem. Phys.* **2020**, *22*, 6538-6552.
41. Iuliano, J. N., et al., Excited State Vibrations of Isotopically Labeled Fmn Free and Bound to a Light-Oxygen-Voltage (Lov) Protein. *J. Phys. Chem. B* **2020**, *124*, 7152-7165.
42. Kitagawa, T.; Nishina, Y.; Kyogoku, Y.; Yamano, T.; Ohishi, N.; Takaisuzuki, A.; Yagi, K., Resonance Raman-Spectra of Carbon-13-Labeled and Nitrogen-15-Labeled Riboflavin Bound to Egg-White Flavoprotein. *Biochemistry* **1979**, *18*, 1804-1808.
43. Copeland, R. A.; Spiro, T. G., Ultraviolet Resonance Raman-Spectroscopy of Flavin Mononucleotide and Flavin Adenine-Dinucleotide. *J. Phys. Chem.* **1986**, *90*, 6648-6654.
44. Quincy, T. J.; Barclay, M. S.; Caricato, M.; Elles, C. G., Probing Dynamics in Higher-Lying Electronic States with Resonance-Enhanced Femtosecond Stimulated Raman Spectroscopy. *J. Phys. Chem. A* **2018**, *122*, 8308-8319.
45. Barclay, M. S.; Caricato, M.; Elles, C. G., Femtosecond Stimulated Raman Scattering from Triplet Electronic States: Experimental and Theoretical Study of Resonance Enhancements. *J. Phys. Chem. A* **2019**, *123*, 7720-7732.
46. Shin, K. S. K.; Zink, J. I., Quantitative Evaluation of the Relationships between Excited-State Geometry and the Intensities of Fundamentals, Overtones, and Combination Bands in Resonance Raman Spectra. *Inorg. Chem.* **1989**, *28*, 4358-4366.
47. Tannor, D. J.; Heller, E. J., Polyatomic Raman Scattering for General Harmonic Potentials. *J. Chem. Phys.* **1982**, *77*, 202-218.
48. Heller, E. J.; Sundberg, R.; Tannor, D., Simple Aspects of Raman Scattering. *J. Phys. Chem.* **1982**, *86*, 1822-1833.
49. Myers, A. B., 'Time-Dependent' Resonance Raman Theory. *J Raman Spectrosc.* **1997**, *28*, 389-401.
50. Myers Kelley, A., Resonance Raman and Resonance Hyper-Raman Intensities: Structure and Dynamics of Molecular Excited States in Solution. *J. Phys. Chem. A* **2008**, *112*, 11975-11991.
51. Albrecht, A. C., On the Theory of Raman Intensities. *J. Chem. Phys.***1961**, *34*, 1476-1484.
52. Heather, R.; Metiu, H., Time-Dependent Theory of Raman Scattering for Systems with Several Excited Electronic States: Application to a H+3 Model System. *J. Chem. Phys.***1989**, *90*, 6903-6915.
53. Wang, X.; Valverde-Aguilar, G.; Weaver, M. N.; Nelsen, S. F.; Zink, J. I., Resonance Raman De-Enhancement Caused by Excited State Mixed Valence. *J. Phys. Chem. A* **2007**, *111*, 5441-5447.
54. Myers, A. B.; Trulson, M. O.; Mathies, R. A., Quantitation of Homogeneous and Inhomogeneous Broadening Mechanisms in Trans-Stilbene Using Absolute Resonance Raman Intensities. *J. Chem. Phys.***1985**, *83*, 5000-5006.
55. Myers, A. B.; Trulson, M. O.; Pardoen, J. A.; Heeremans, C.; Lugtenburg, J.; Mathies, R. A., Absolute Resonance Raman Intensities Demonstrate That the Spectral Broadening Induced by the B-Ionone Ring in Retinal Is Homogeneous. *J. Chem. Phys.***1986**, *84*, 633-640.
56. Hall, C. R.; Conyard, J.; Heisler, I. A.; Jones, G.; Frost, J.; Browne, W. R.; Feringa, B. L.; Meech, S. R., Ultrafast Dynamics in Light-Driven Molecular Rotary Motors Probed by Femtosecond Stimulated Raman Spectroscopy. *J. Am. Chem. Soc.* **2017**, *139*, 7408-7414.
57. Heisler, I. A.; Moca, R.; Camargo, F. V. A.; Meech, S. R., Two-Dimensional Electronic Spectroscopy Based on Conventional Optics and Fast Dual Chopper Data Acquisition. *Rev. Sci. Instrum.* **2014**, *85*, 10.
58. Frisch, M. J., et al., Gaussian 09, Revision B.01. Wallingford CT, 2009.
59. Scalmani, G.; Frisch, M. J.; Mennucci, B.; Tomasi, J.; Cammi, R.; Barone, V., Geometries and Properties of Excited States in the Gas Phase and in Solution: Theory and Application of a Time-Dependent Density Functional Theory Polarizable Continuum Model. *J. Chem. Phys.***2006**, *124*, 094107.

60. Tomasi, J.; Mennucci, B.; Cammi, R., Quantum Mechanical Continuum Solvation Models. *Chem.Rev.* **2005**, *105*, 2999-3094.
61. Becke, A. D., Density-Functional Thermochemistry. Iii. The Role of Exact Exchange. *J. Chem. Phys.***1993**, *98*, 5648-5652.
62. Lee, C.; Yang, W.; Parr, R. G., Development of the Colle-Salvetti Correlation-Energy Formula into a Functional of the Electron Density. *Phys. Rev. B* **1988**, *37*, 785-789.
63. Wetmore, S. D.; Huang, Y., Looking Back on 90 Years of the Canadian Journal of Chemistry. *Can. J. Chem.* **2019**, *97*, iii-iv.
64. Zenichowski, K.; Gothe, M.; Saalfrank, P., Exciting Flavins: Absorption Spectra and Spin–Orbit Coupling in Light–Oxygen–Voltage (Lov) Domains. *J Photochem Photobiol A Chem* **2007**, *190*, 290-300.
65. Brealey, G. J.; Kasha, M., The Role of Hydrogen Bonding in the N- Pi-Star Blue-Shift Phenomenon. *J. Am. Chem. Soc.* **1955**, *77*, 4462-4468.
66. Lu, T.; Chen, F., Multiwfn: A Multifunctional Wavefunction Analyzer. *J. Comput. Chem.* **2012**, *33*, 580-592.
67. Kucharski, S. A.; Włoch, M.; Musiał, M.; Bartlett, R. J., Coupled-Cluster Theory for Excited Electronic States: The Full Equation-of-Motion Coupled-Cluster Single, Double, and Triple Excitation Method. *J. Chem. Phys.***2001**, *115*, 8263-8266.
68. Korona, T.; Werner, H.-J., Local Treatment of Electron Excitations in the Eom-Ccsd Method. *J. Chem. Phys.***2003**, *118*, 3006-3019.
69. Rishi, V.; Perera, A.; Nooijen, M.; Bartlett, R. J., Excited States from Modified Coupled Cluster Methods: Are They Any Better Than Eom Ccsd? *J. Chem. Phys.***2017**, *146*, 144104.
70. NIST Nist Standard Reference Database Number 101. 2020; Https://Cccbdb.Nist.Gov/Vibscalejust.Asp. https://cccbdb.nist.gov/vibscalejust.asp (accessed 4-13-21).
71. Schmidt, J.; Coudron, P.; Thompson, A. W.; Watters, K. L.; McFarland, J. T., Hydrogen Bonding between Flavin and Protein: A Resonance Raman Study. *Biochemistry* **1983**, *22*, 76-84.
72. Petrenko, T.; Neese, F., Analysis and Prediction of Absorption Band Shapes, Fluorescence Band Shapes, Resonance Raman Intensities, and Excitation Profiles Using the Time-Dependent Theory of Electronic Spectroscopy. *J. Chem. Phys.***2007**, *127*, 164319.
73. Kim, H.; Kosuda, K. M.; Van Duyne, R. P.; Stair, P. C., Resonance Raman and Surface- and Tip-Enhanced Raman Spectroscopy Methods to Study Solid Catalysts and Heterogeneous Catalytic Reactions. *Chem. Soc. Rev.* **2010**, *39*, 4820-4844.

ToC Graphic

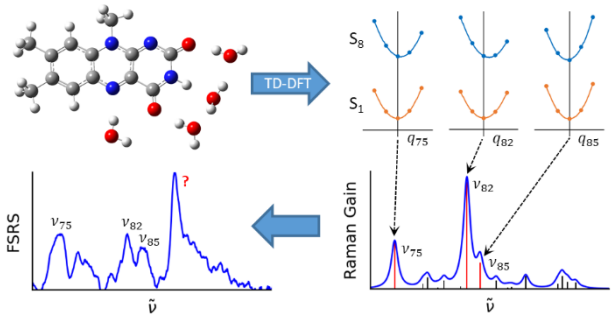
TD-DFT
S8
S1
q75
q82
q85
ν82
ν75
ν85
Raman Gain
FSRS
?
ν75
ν82
ν85
ν̃
ν̃